Axial segregation in a cylindrical centrifuge

Jonghoon Lee and Anthony J. C. Ladd*
Chemical Engineering Department, University of Florida, Gainesville, Florida 32611-6005
(Dated: April 18, 2002)

We propose a theory for axial segregation of suspensions of non-neutrally buoyant particles in a rotating cylinder. We show that the hydrodynamic interaction between pairs of particles produces a relative motion in the axial direction, independent of the gravitational force. If the particles are denser than the suspending fluid, differential centrifuging between particles at different radial positions leads to an attractive interaction, inducing a rapid growth of axial density perturbations. We suggest that this mechanism can explain the origin of band formation in rotating suspensions of non-neutrally buoyant particles.

PACS numbers: 45.70.Qj, 47.15.Gf, 82.70.Kj, 83.10.Pp

A homogeneous suspension of non-neutrally buoyant particles in a rotating cylinder can be unstable to axial perturbations in concentration. In a recent experiment [1], dilute suspensions of non-Brownian silica particles, radius $a = 100\,\mu$m and specific gravity $\rho_s/\rho_f \simeq 2$, were suspended in glycerol-water mixtures up to 100 times as viscous as water. After a few hundred rotations of the cylinder, typically at an angular velocity of $\Omega \sim 1\,$rad/sec, density fluctuations along the symmetry axis were observed, eventually leading to well defined bands of high and low particle concentration. Similar experiments with neutrally buoyant particles do not show any axial segregation unless the cylinder is only partially filled [2]. A mechanism for axial segregation in the presence of a free surface was recently proposed, based on shear-induced diffusion of the particles [3]. In this paper, we develop a theory for a filled cylinder, which predicts segregation when the particles are denser than the solvent. The theory has no adjustable parameters, yet the calculated growth rate of the most unstable mode is consistent with the band onset times observed experimentally.

The theory is limited to dilute suspensions, and thus the particle trajectories were derived from the dynamics of an isolated particle in a rotational flow. The hydrodynamic interaction between a pair of particles was then calculated by the method of reflections, taking only the leading-order terms. We found a small relative velocity between the particles, which is always attractive, and which eventually leads to axial segregation. However, to a first approximation, the effect of hydrodynamic interactions on the particle trajectories can be ignored in comparison with the much larger rotational flow. This assumption is reasonable if the angular velocity of the cylinder is much greater than the rate of axial segregation, which turns out to be true under the conditions of the experimental observations.

An isolated particle located on a cross section of the rotating cylinder at $\mathbf{r} = (r, \theta)$, experiences a gravitational force $-m_B g\hat{\mathbf{j}}$ and a centrifugal force $m_B\Omega^2 r\hat{\mathbf{r}}$ (Fig. 1(a)), where $m_B = 4/3\,\pi a^3(\rho_s - \rho_f)$ is the buoyancy corrected mass of the particle. In isolation these forces give rise to a settling velocity $-u_s\hat{\mathbf{j}}$, where $u_s = m_B g/6\pi\mu a$, and a centrifuging velocity $u_c(r/R)\hat{\mathbf{r}}$, where $u_c = m_B\Omega^2 R/6\pi\mu a$. For the range of experimental parameters where band formation is observed (viscosity $\mu > 10\,$cp and angular velocity $\Omega < 3\,$rad/s), the Stokes number for settling ($St_s = \rho_s u_s a/\mu < 10^{-1}$) and for centrifuging ($St_c = \rho_s u_c a/\mu < 10^{-3}$) are both small. Inertia can therefore be neglected in these calculations and the particle velocity determined from the instantaneous force balance. The velocity $\mathbf{u}$ of an isolated particle located at $\mathbf{r}$ is then,

$$u_r = u_s\left(\frac{r}{D_1 R} - \sin\theta\right), u_\theta = u_s\left(\frac{r}{D_2 R} - \cos\theta\right), \quad (1)$$

where $D_1 = g/\Omega^2 R = u_s/u_c$ and $D_2 = u_s/\Omega R$ are two independent dimensionless numbers describing the relative magnitudes of the three forces (gravitational, centrifugal, and Stokes drag) acting on the particle. The effect of the cylinder wall on the particle dynamics is neglected here, although we subsequently consider the screening of the hydrodynamic interactions by the cylinder wall. Equating u_r and u_θ to zero yields two circles (centers C_1 and C_2) with diameters of $D_1 R$ and $D_2 R$, on which velocity components vanish (Fig. 1(b)). Usually a particle follows the local stream velocity, but it goes against the stream inside the circle C_2, where the downward gravitational force is larger than the upward drag force. Similarly, a particle usually migrates toward the cylinder wall, but moves towards the central axis inside the circle C_1, where the downward gravitational force is larger than the upward centrifugal force. The intersection of these circles (P) is a point of unstable equilibrium, where all three forces balance, and is the dynamical center of this system. A particle initially placed near this point will spiral outwards, eventually ending up with a limiting closed trajectory determined by the cylinder wall (Fig. 1(c)). A qualitative prediction of the limiting trajectories of a single particle can be made based on the size of these circles within a finite radius cylinder. For example, if $D_2 > 1$ a particle cannot have a closed trajectory; instead it moves

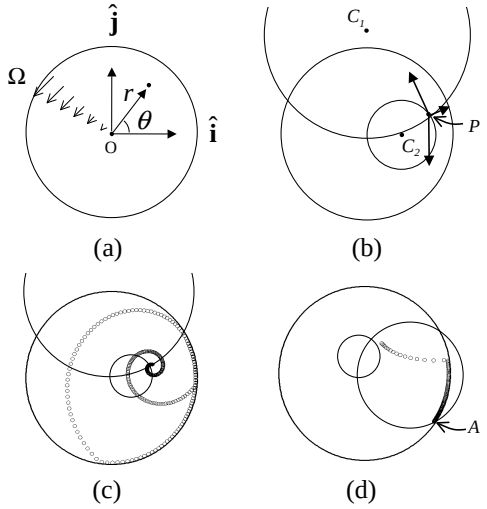

FIG. 1: Characterization of isolated particle dynamics: (a) the coordinate system used in Eq. 1; (b) Circles C_1 and C_2 describe the locus of points of zero radial and angular velocity; (c) spiral motion of a single particle placed near the unstable equilibrium point, P; (d) when $D_2 > 1$, a particle cannot have closed trajectory.

directly towards the point A in less than 1 period, which is the lower intersection between the circle C_2 and the cylinder wall (Fig. 1(d)). In the case of a dilute suspension under slow rotation ($D_2 > 1$), the particles will congregate in a dense pack near this intersection point. The particles used in the laboratory experiments have a Stokes velocity $u_s \sim 3\,\mathrm{cm/s}$ in water, so that the rotational period must be less than 2 s to avoid stagnation; otherwise there is insufficient viscous drag to overcome the gravitational force on the particles. This represents the upper limit of the angular velocity in the experiments performed to date, so it is unsurprising that band formation was not observed unless the the suspending fluid was more viscous. Our theory is only valid for homogeneous suspensions, and so excludes the case where $D_2 > 1$.

Under the experimental conditions where band formation is observed, $D_1 \sim 10^3$ and $D_2 \sim 10^{-2}$. Because the radius of C_1 is so large, while that of C_2 is so small, the unstable equilibrium point, P, is almost exactly on the $\hat{\mathbf{i}}$ axis, displaced from the center of the cylinder by $D_2 R$; *i.e.* $\mathbf{r}(P) = (D_2 R)\hat{\mathbf{i}} + \mathcal{O}(D_2^2 R/D_1)\hat{\mathbf{j}}$ (see Fig. 2(a)). The velocity of a particle relative to the stream,

$$\frac{\mathbf{v}}{\Omega R} = \frac{\mathbf{u} - \Omega r\hat{\theta}}{\Omega R} = D_2\left(\frac{\mathbf{r}}{D_1 R} - \hat{\mathbf{j}}\right), \qquad (2)$$

has a small centrifuging component in addition to the much larger settling velocity. Nevertheless, it will be shown that it is the centrifugal velocity u_c that leads to band formation. As the particle rotates in a nearly circular orbit about P (dashed line in Fig. 2(a)), it is continuously falling from the local stream line (dotted lines in Fig. 2(a)). The circular orbit is perturbed by

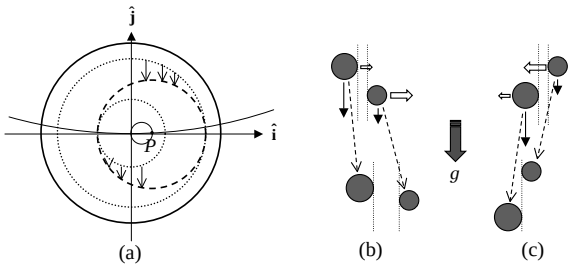

FIG. 2: (a) Single particle trajectory neglecting centrifugal migration. (b, c) Relative velocity of two particles sedimenting with different settling velocities: (b) when the particle behind falls faster than the particle in front, they repel each other; (c) when the particle in front falls faster, they attract.

the weak centrifugal velocity, u_c, and the particle eventually approaches the limiting closed trajectory, but with a very long time scale $\sim D_1/D_2\Omega$. Thus for the purpose of determining the onset of the axial instability, it will be assumed that the suspension is homogeneous in the transversal plane.

Next we consider the hydrodynamic interaction between two identical particles with positions $\mathbf{R}_i = (\mathbf{r}_i, z_i)$, where $\mathbf{r}_i = (r_i, \theta_i)$ and z_i is the axial position, again ignoring wall effects. If the particles are moving with velocities $\mathbf{v}_1$ and $\mathbf{v}_2$ relative to the stream velocity $\mathbf{\Omega} \times \mathbf{r}$ (Eq. 2), then the leading order correction to the particle velocity can be found by the method of reflections [4]. The relative velocity then contains an axial component, which is absent in Eq. 2;

$$v_{12,z} = -\frac{3au_c}{4R}\frac{z\mathrm{r}_{12}^2}{\mathrm{R}_{12}^3}, \qquad (3)$$

where $v_{12,z} = [\mathbf{v}_2 - \mathbf{v}_1]_z$, $\mathrm{r}_{12} = |\mathbf{r}_2 - \mathbf{r}_1|$, $\mathrm{R}_{12} = |\mathbf{R}_2 - \mathbf{R}_1|$ and $z = z_2 - z_1$. Equation (3) implies that the hydrodynamic interaction in a rotating cylinder between particles that are denser than the suspending medium is always attractive, and will thus provoke instabilities in the concentration profile. This can be understood by an analogy between centrifuging and sedimentation. It is well known that there is relative motion along the horizontal direction when two particles are sedimenting with different settling velocities (Fig. 2(b, c)). Centrifuging can be interpreted as a sedimentation process driven by a force proportional to the radial position of the particle, which means that the particle closest to the cylinder wall always moves faster. This differential centrifugal force between particles at different radial positions induces an attractive motion along the axial direction of the cylinder, independent of the gravitation force and regardless of the location of the particles in the transversal plane. However, the relative velocity of the pair is small in comparison to both the radial migration velocity $u_c r/R$ of a single particle and the relative radial migration of the pair $u_c \mathrm{r}_{12}/R$. Thus this migration is of primary signifi-

cance in the axial direction, where there is otherwise no relative motion.

These conclusions are quantitatively though not qualitatively affected by the presence of the cylinder wall. The lubrication force between a particle and the cylinder wall reduces the radial velocity when the particle comes in close proximity to the wall [5]. This in turn reduces the differential centrifuging driving the axial attraction and in some instances can change the attraction to a weak repulsion, since it is now possible for the inner particle to centrifuge faster than the outer one. However the strongest effect of the lubrication force is restricted to particles within one or two radii of the wall and thus the overall effect on bulk properties is negligible for sufficiently large cylinders, at least at low particle concentrations. On the other hand the cylinder wall also screens the hydrodynamic interaction between particles that are far apart relative to the cylinder radius [6]. Wall screening is independent of the cylinder size and is therefore more important than the lubrication force.

Wall screening can be approximated to first order in the inverse separation by using image particles. The image of particle i is located on the opposite side of the cylinder wall, $\mathbf{R}_{i'} = (2R - r_i, \theta_i, z_i)$ with instantaneous velocity $\mathbf{v}_{i'} = -\mathbf{v}_i$. Based on the linearity of the Stokes equation, The relative axial velocity including wall screening, $w_{12,z}$, is therefore

$$\begin{aligned} w_{12,z} = v_{12,z} \;&+\; \frac{3az}{4}\left[u_c\left(\frac{\mathbf{r}_{12'}\cdot\mathbf{r}_2}{R\mathrm{R}_{12'}^3} - \frac{\mathbf{r}_{1'2}\cdot\mathbf{r}_1}{R\mathrm{R}_{1'2}^3}\right)\right] \\ &-\; \frac{3az}{4}\left[u_s\left(\frac{\mathbf{r}_{12'}}{\mathrm{R}_{12'}^3} - \frac{\mathbf{r}_{1'2}}{\mathrm{R}_{1'2}^3}\right)\cdot\hat{\mathbf{j}}\right]. \end{aligned} \tag{4}$$

The additional terms on the right hand side describe the effects of screening on the centrifuging velocity and the settling velocity, respectively.

The effect of an axial drift velocity on the particle concentration $c(z,t)$ can be obtained from the mass balance,

$$\partial_t c(z,t) = -\partial_z \int_{-\infty}^{\infty} c(z,t)\langle w_{12,z}(z-z')\rangle c(z',t)\pi R^2\, dz', \tag{5}$$

where $c(z',t)\pi R^2\, dz'$ is the number of particles in an axial slice dz' located at z'. An infinite cylinder length is assumed so that end effects can be neglected, and $\langle w_{12,z}(z)\rangle$ is the spatial average over the (r, θ) plane of the relative velocity of pairs of particles separated axially by z;

$$\langle w_{12,z}(z)\rangle = \frac{2}{\pi R^4}\int_0^R\int_0^R\int_0^{2\pi} dr_1 dr_2 d\theta\; r_1 r_2 w_{12,z}(z), \tag{6}$$

where $\theta = \theta_2 - \theta_1$. Notice that $\langle w_{12,z}(z)\rangle$ is independent of the gravitational force, because the gravitational contribution to $w_{12,z}(z)$ (Eq. 4) averages to zero. A homogeneous distribution of particles in the (r, θ) plane has been assumed in the averaging, but the suspension

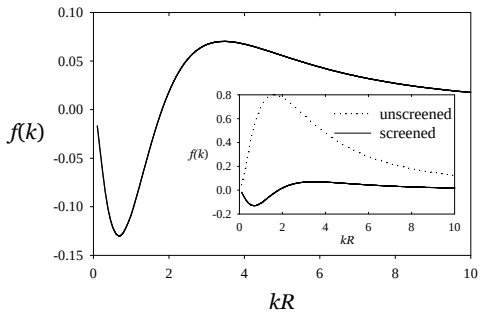

FIG. 3: $f(k)$ is plotted against kR. The dotted line in the capsulated figure is Eq. 10.

is initially in a highly non-uniform state, with particles in a dense pack at the bottom of the cylinder. Even after some startup time the particles may not be distributed uniformly in the transversal plane, as assumed in Eq. 6. Nevertheless we do not expect our conclusions to be sensitive to radial variations in particle concentration, since all direct interactions, $v_{12,z}$, are attractive and long ranged.

We now consider the stability of a small sinusoidal perturbation to the concentration field, $c(z,t) = c_0 + c_k(t)e^{ikz}$. Linearizing Eq. 5 yields exponentially growing instabilities when

$$w_k = \int_{-\infty}^{\infty} dz\, e^{-ikz}\frac{d\langle w_{12,z}(z)\rangle}{dz} < 0. \tag{7}$$

The growth rate of each mode is given by

$$\begin{aligned} \gamma_k &= -c_0\pi R^2 w_k \\ &= \frac{\phi(\rho_s-\rho_f)\Omega^2 R^2}{8\mu} f(k), \end{aligned} \tag{8}$$

where ϕ is the particle volume fraction and $f(k)$ contains the wavelength dependence of the growth rate. The expression for $f(k)$ is a four dimensional integral over r_1, r_2, θ, and z, and after integrating by parts,

$$f(k) = \int_{-\infty}^{\infty} dz\, k\sin(kz)\left\{\left\langle\frac{z\mathrm{r}_{12}^2}{\mathrm{R}_{12}^3}\right\rangle - 2\left\langle\frac{z\mathbf{r}_{12'}\cdot\mathbf{r}_2}{\mathrm{R}_{12'}^3}\right\rangle\right\}. \tag{9}$$

The integral over z can be expressed in terms of the modified Bessel function K_0 [7], reducing the expression to spatial averages of the form given in Eq. 6. The Bessel functions $K_0(k\mathrm{r}_{12})$ and $K_0(k\mathrm{r}_{12'})$ can be expanded as products of functions of r_1, r_2, and θ [8] and the resulting integrals written in terms of modified Bessel functions of the 1st and 2nd kind [7]:

$$f_0 = 16\left[2K_2I_2 - K_0I_2 - K_1I_1\right], \tag{10}$$

and

$$\begin{aligned} f_1(k) &= 16I_0(k)\left[K_2(k) + 4k^{-1}\left(K_i(k) - K_1(2k)\right)\right] \\ &- 16I_1(k)\left[8K_1(2k) - 8K_3(2k) + K_3(k)\right] \\ &- 64I_1(k)k^{-1}\left[4K_0(2k) - K_0(k) + 3k^{-1}K_i(k)\right], \end{aligned} \tag{11}$$

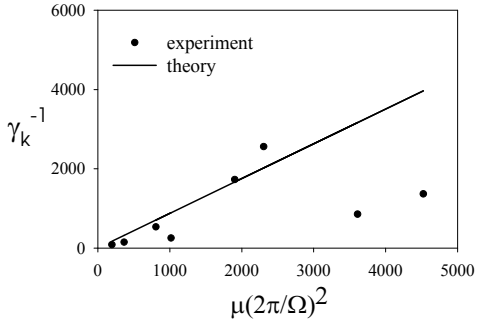

FIG. 4: Band onset time observed experimentally is compared with mode growth rate γ_k^{-1} of the most unstable mode.

where

$$K_i(k) = -\int_k^{2k} dt\, K_0(t). \tag{12}$$

Here $f_0(k)$ is the bulk contribution, $f_1(k)$ is the correction due to the wall screening, and $f(k) = f_0(k) + f_1(k)$. We have checked the expressions in Eqs. 10 and 11 by also evaluating the integrals in Eq. 9 numerically.

Evaluating $f(k)$ shows that the fastest growing mode has a wave number $k = 3.5/R$ (Fig. 3) and a wavelength $\lambda = 1.8R$, which is close to the experimentally observed spacing between the bands. On the other hand, if hydrodynamic screening is neglected, then $f(k) = f_0(k)$ and the most unstable mode has a longer wavelength $\lambda = 3.9R$ (Fig. 3). It can be seen that the long wavelength ($\lambda > 3R$) modes are stable for screened interactions, but unstable in the unscreened case. This happens because the image particles outside the wall make a larger angle with the z-axis, so the repulsive image interaction can be larger than the attractive direct interaction at small k. We have not been able to check the accuracy of the image-particle approximation for a cylindrical wall, as opposed to a planar boundary, so the precise shape of $f(k)$ is uncertain at present.

An experimental realization of axial segregation without hydrodynamic screening might be achieved in a microgravity environment, by partially filling a central core (radius R_1) of the cylinder with suspension and leaving an annulus of pure fluid outside, so that

$$c(z,0) = \begin{cases} c_0 & : \quad r < R_1 \\ 0 & : \quad R_1 < r < R \end{cases} . \tag{13}$$

As long as the cylinder is only about half filled ($R_1 < R/2$), hydrodynamic screening should be negligible. Although radial migration and dispersion would make R_1 weakly time dependent, we would expect a much stronger axial segregation than for a filled cylinder, with about double the separation between the bands ($\simeq 4R_1$).

We were surprised to discover that the initial segregation process is driven solely by differential centrifuging, although gravity may play a role in the later stages of band formation, when there are substantial inhomogeneities in particle concentration. In Fig. 4, the band onset time observed experimentally is compared with the mode growth time γ_k^{-1} of the most unstable mode. The band onset time was determined by measuring the time delay between cylinder startup and the first appearance of bands in the concentration profile. Our theory predicts that the band growth rate is proportional of Ω^2/μ (Eq. 8). Although there is large scatter in the experimental data, the band onset time is roughly proportional to $\mu\Omega^{-2}$ over a range of viscosities ($10 - 70$ cp) and rotation periods ($1 - 10$ Hz). Moreover, with the exception of 2 outlying points, the experimental data is consistent with the predicted values of γ_k, but a quantitative comparison awaits more precise measurements of the growth rate.

In this work, we have proposed a theory for axial segregation of a non-neutrally buoyant particle suspension in a rotating cylinder. The main idea is that the differential centrifuging at different radial positions drives an axial attraction between pairs of particles, which amplifies any existing concentration fluctuation. Our theory is consistent with the band width and the band onset time observed experimentally, and has no adjustable parameters. We note that in a suspension of particles that are less dense than the suspending medium, any axial perturbation in concentration will decay due to stabilizing repulsive interactions. In a suspension of neutrally buoyant particles, centrifuging is absent and the suspension is stable in the absence of a free surface [2].

We thank Bruce Ackerson and Penger Tong for introducing us to this problem and for providing data prior to publication.

* Electronic address: ladd@che.ufl.edu; URL: http://ladd.che.ufl.edu

[1] W. R. Matson, B. J. Ackerson, and P. Tong, Phys. Rev. Lett (2002), preprint LR8443.
[2] M. Tirumkudulu, A. Mileo, and A. Acrivos, Phys. Fluids **12**, 1615 (2000).
[3] R. Govindarajan, P. R. Nott, and S. Ramaswamy, Phys. Fluids **13**, 3517 (2001).
[4] H. Brenner J. Fluid Mech. **18**, 144 (1964).
[5] J. Happel,and H. Brenner, *Low Renolds Number Hydrodynamics* (Prentice-Hall, Inc., Eaglewood Cliffs. N.J., 1965).
[6] M. P. Brenner Phys. Fluids **11**, 754 (1999).
[7] M. Abramowitz, *Handbook of Mathematical functions* (Dover Publications, Inc., Washington, D.C., 1972).
[8] J. D. Jackson, *Classical Electrodynamics* (John Wiley & Sons, Inc., New York, 1998).